# NOTES AND CORRESPONDENCE

## Dual-Doppler Analysis of Winds and Vorticity Budget Terms near a Tornado

JOSHUA WURMAN

*Center for Severe Weather Research, Boulder, Colorado*

YVETTE RICHARDSON

*The Pennsylvania State University, University Park, Pennsylvania*

CURTIS ALEXANDER

*School of Meteorology, University of Oklahoma, Norman, Oklahoma*

STEPHEN WEYGANDT

*National Oceanic and Atmospheric Administration/Earth System Research Laboratory, Boulder, Colorado*

PENG FEI ZHANG

*Cooperative Institute for Mesoscale Meteorological Studies, University of Oklahoma, Norman, Oklahoma*

(Manuscript received 5 July 2006, in final form 15 September 2006)

ABSTRACT

Three-dimensional dual-Doppler observations with unprecedented finescale spatial and temporal resolution are used to characterize the vector wind field and vorticity generation terms in and near a weak, short-lived tornado. The beam widths of the two Doppler on Wheels (DOW) mobile radars, at the range of the tornado, are 250 m with gate lengths of 75 m, resulting in a resolution of less than $10^7$ $m^3$. One of the DOWs collected data during the 240 s prior to the formation of the tornado, enabling examination of the genesis process. A single set of volumetric scans suitable for dual-Doppler analyses were completed by both DOWs, permitting the calculation of vertical and horizontal vorticity, divergence, and stretching and tilting terms in the vorticity budget of the large but weak tornado and its surroundings, but no local tendency terms. Analyses of the dual-Doppler vector wind fields document, for the first time in a supercellular tornado, revealed several structures expected to be associated with tornadoes, including the tilting of horizontal vorticity into the vertical near the tornado, and stretching of vertical vorticity in the region of the tornado. The analyses are compared to conceptual and computer models of tornadic storms, confirming the existence of various phenomena and processes, although some model predictions, particularly those concerning the distribution of horizontal vorticity, could not be verified through these analyses. The observed magnitudes of stretching of vertical vorticity and tilting of horizontal vorticity are consistent with those necessary for generating the observed vorticity near the tornado.

### 1. Introduction

Conceptual models of supercell storm structure based upon visual observations since the 1950s include features such as the forward- and rear-flank downdrafts, inflow notches, updrafts, and the gust fronts that delineate the boundaries of air masses that have been processed by a convective updraft or downdraft with those that have not (Stout and Huff 1953; Ludlam 1963; Fujita 1975; Lemon and Doswell 1979). Tornadoes are believed to develop along such gust fronts, which also coincide with the interface between an updraft and a downdraft in the parent supercell.

Numerical simulations of supercells conducted in the

*Corresponding author address:* Joshua Wurman, Center for Severe Weather Research, 1945 Vassar Circle, Boulder, CO 80305. E-mail: jwurman@cswr.org

DOI: 10.1175/MWR3404.1

1980s, 1990s, and 2000s have reproduced many of the features in the conceptual model of a supercell including tornado-like vortices. However, these simulations have raised more questions about the mechanisms by which tornadoes are formed and maintained, and these results have not been confirmed by high-resolution observations (Wicker and Wilhemson 1995; Klemp et al. 1981; Adlerman et al. 1999; Adlerman 2003; Klemp and Rotunno 1983; Wicker et al. 2002; Romine et al. 2004; Xue 2004). The tilting of horizontal vorticity and its association with tornadoes has been inferred but not verified. The role of the rear-flank downdraft in the generation of vertical vorticity at low levels, the subsequent occlusion of the tornadic circulation, and the distribution of circulation with height predicted in these simulations require verification through analysis of observations. Dual-Doppler observations of sufficient resolution to assess these fields, particularly those that appear in equations relating to vorticity generation and maintenance, have been lacking.

Coincident with the maturation of numerical simulations was the development of observational tools such as airborne, stationary, and mobile ground-based Doppler weather radar and mobile surface observations, which permitted more frequent sampling of supercell and tornado structures at close range and yielded the necessary resolution to detect storm-scale features on the order of 500–1000 m (Ray et al. 1975, 1981; Brandes 1977, 1978, 1981, 1984a; Fujita and Wakimoto 1982; Brandes et al. 1988; Dowell and Bluestein 1997, 2002a,b; Wakimoto and Liu 1998; Wakimoto and Cai 2000; Bluestein and Gaddy 2001; Klemp et al. 1981; Rasmussen et al. 1982; Jensen et al. 1983; Markowski et al. 2002; Bluestein and Pazmany 2000; Bluestein et al. 2003, 2007; Burgess et al. 2002; Richardson et al. 2001; Wurman and Alexander 2005). However, conventional Doppler weather radar has the major limitation of permitting the observation of only one component of the full 3D wind field. This limitation necessitated more sophisticated radar scanning strategies for airborne radar or the deployment of multiple ground-based mobile radars in order to observe more than a single component of the wind, and permit the analysis of a full 3D vector wind field through a dual-Doppler synthesis (e.g., Dowell and Bluestein 2002a,b). However, the region within about 1 km AGL is poorly sampled by many of these radar systems due to ground clutter returns and/or the radar horizon, and/or large sampling volumes prohibit the resolution of boundary layer features less than roughly 500 m in scale. These critical features include near-surface convergence and divergence along with the distribution of horizontal and vertical vorticity in or near supercell tornadoes. Dual-Doppler analyses of nonsupercell tornadoes (Roberts and Wilson 1995) have been conducted, but it is likely that the dynamics of the genesis and maintenance of supercell-spawned tornadoes differ significantly.

The Doppler on Wheels (DOW) radars (Wurman et al. 1997; Wurman 2001) collected observations for the first high-resolution (data spacing of 250 m $\times$ 250 m $\times$ 75 m) dual-Doppler analysis during field operations in the spring of 1997 (Wurman et al. 2007a). However, radar observations by both radars were collected at only a single elevation, permitting the synthesis of the wind field at only one horizontal level. This prohibited the estimation of dynamical quantities requiring vertical derivatives such as vortex stretching and tilting, which are involved in the production and maintenance of vertical vorticity in the lowest levels of a supercell and, presumably, a tornado.

In the spring of 1998, the DOWs intercepted a supercell in western Nebraska near the town of Bridgeport, and the radars were able to establish a brief high-resolution dual-Doppler observation of a tornado at multiple levels for the first time.

## 2. Mesoscale evolution

Just after 0000 UTC 21 May 1998, a supercell was observed by the Cheyenne, Wyoming, National Weather Service radar (KCYS) at a range of 140–150 km (Fig. 1). The mesocyclone detection algorithm from KCYS reports a shear value of 0.019 $s^{-1}$ in this supercell at 0037 UTC, which is a maximum for the 1-h observation period between 0000 and 0100 UTC. Just after 0042 UTC the storm continues to exhibit the radar characteristics of a mature supercell with a well-defined hook and sharp reflectivity gradients along its forward flanks (Fig. 1b). A minimum in reflectivity is also noted downstream of the forward core, and reflectivities in the hook echo now exceed 60 dB$Z$. The supercell reflectivity structure maintains its appearance until after 0100 UTC when new convection approaches the storm from the southwest.

The low-elevation Doppler-velocity presentation of the supercell is often incomplete as the hook echo is located at a great range from KCYS. The large range and the elevation differences due to terrain place the height of the lowest beam about 3.7 km AGL in the supercell. Furthermore, 3-dB radar beamwidths at this range are about 2.8 km wide resulting in very poor spatial resolution within the storm. However, the

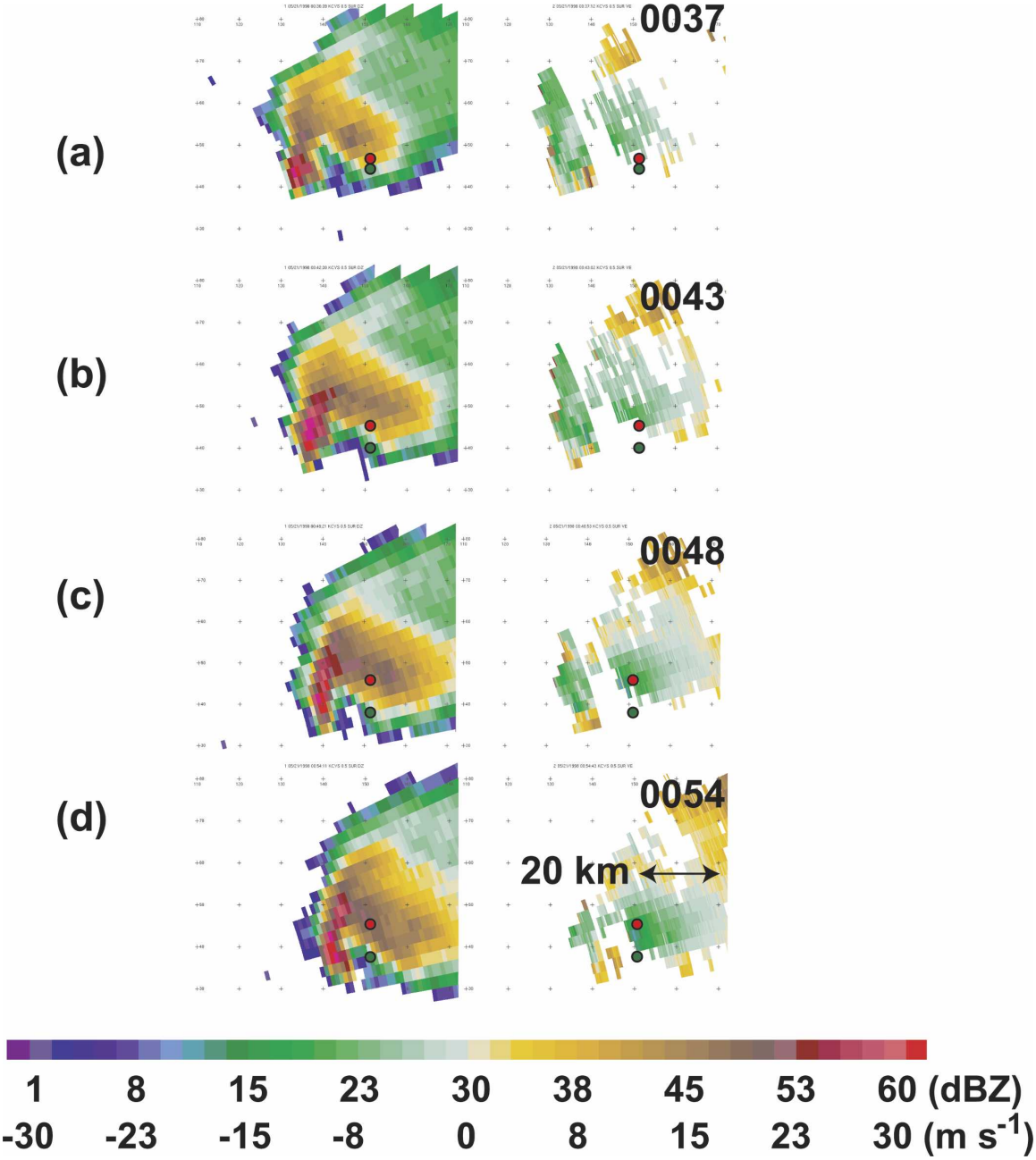


FIG. 1. The 0.5° elevation scan of a supercell from KCYS [located well off the lower-left corner of (a)–(d) at a range of 140–150 km] showing both (left) base reflectivity and (right) Doppler velocity on 21 May 1998 at the times indicated. The locations of DOW2 (red circles) and DOW3 (green circles) at each time are indicated.

KCYS data do provide an important context for the higher-resolution DOW observations.

Local law enforcement officials reported a tornado 11 miles southeast of Bridgeport from 1758 to 1804 Mountain Standard Time (MST; 0058–0104 UTC; NCDC 1998). The location and time of this report do not agree well with those of the tornado observed in this study, but sometimes these reports contain errors in these quantities. The tornado is listed as F1 (Fujita 1975), but no damage is described in the official report.

## 3. DOW observations of the supercell and tornado

To obtain dual-Doppler data, the crews of the DOWs attempted to deploy in an approximate north–south baseline arrangement ahead of the expected path of the

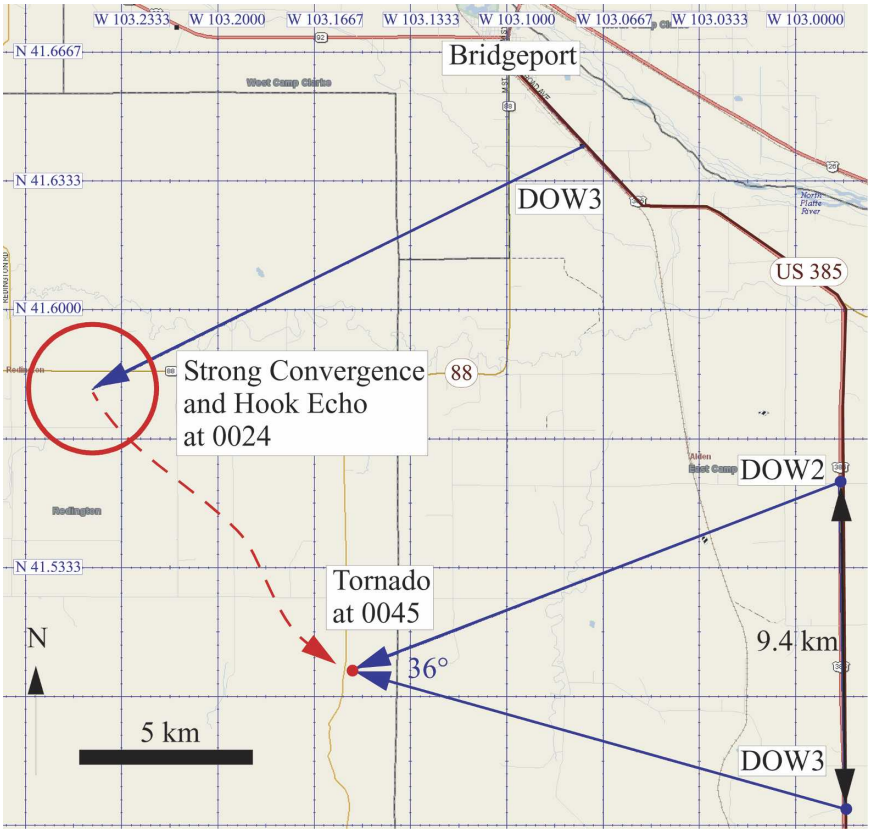


FIG. 2. Location of radars at 0024 UTC 21 May 1998 for single-Doppler observation of pretornadic region (circle) and 0045 UTC dual-Doppler deployment of tornado (at intersection of blue line segments).

supercell (Fig. 2). The DOW2 radar deployed, leveled precisely, and began collecting data at 0040:30 UTC as the DOW3 radar drove south to its eventual deployment site. Thus, during the period from 0040 to 0045 UTC, only single-Doppler data are available.

At 0040 UTC, a prominent anticyclonic flare extended from the tip of the hook echo throughout the observed depth of the hook echo region (70–5000 m AGL; Fig. 3). A broad region of implied cyclonic rotation existed near the surface (Fig. 4) with peak Doppler velocities of only 20 m $s^{-1}$ extending over a 3 × 5 km area. Peak cyclonic vorticity, as estimated from $2\Delta V/\Delta x$ across the circulation, where $V$ is the magnitude of the Doppler velocity and $\Delta x$ is the distance across the circulation, was 0.06 $s^{-1}$ below 200 m AGL (Fig. 5), which is substantially less than that typically associated with tornadoes observed by DOWs (Wurman et al. 1996; Wurman and Gill 2000; Alexander and Wurman 2005; Wurman 2002; Lee and Wurman 2005; Wurman et al. 2007b). Clearly, no tornado is present at this time. To the south of this area, implied anticyclonic flow is associated with the anticyclonic reflectivity flare. Intense inbound Doppler velocities and convergence are present above 3 km AGL, suggestive of a strong rear-flank downdraft (Lemon and Doswell 1979) associated with the anticyclonic reflectivity flare.

From 0040 to 0043 UTC the convergence aloft and the magnitude of the inbound Doppler velocities weaken, suggesting that the downdraft has weakened. The portion of the hook echo west of the anticyclonic flare begins to curve more cyclonically near the surface, while the structure aloft becomes disorganized. No tight circulation exists before 0044:33 UTC either near the ground or aloft. Vertical vorticity remains generally below 0.1 $s^{-1}$ at all observed levels until 0044:33 UTC (Fig. 5).

Dramatic change occurs at 0044 UTC. Vertical vorticity increases to 0.16–0.25 $s^{-1}$ in the 0–1000 m AGL region as a tight circulation, indicative of a weak tornado, forms near the ground. Peak velocities increase to 35 m $s^{-1}$ by 0045:46 UTC associated with a vertical vorticity of 0.52 $s^{-1}$. The circulation is much broader from 1 to 4 km AGL, with vertical vorticities below 0.1 $s^{-1}$. At 5 km AGL an intense and tight circulation

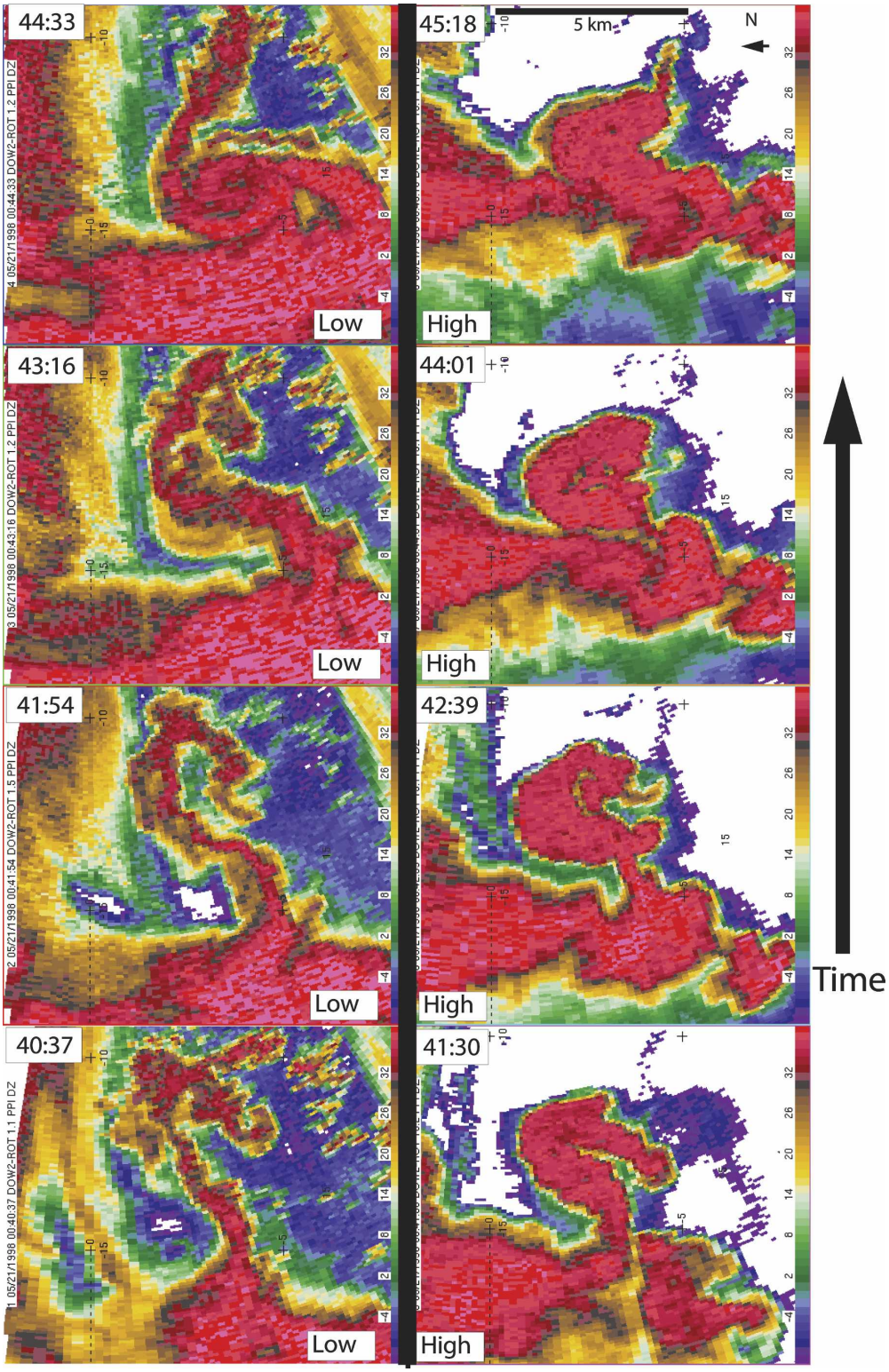


FIG. 3. Low-level and midlevel evolution of the hook echo during tornadogenesis. Scans through the developing tornado at approximately (left) 1.2°–1.5° and (right) 13°–16° elevation reveal both a cyclonically tipped hook echo and an anticyclonic flare during the 300 s prior to tornado formation and the dual-Doppler deployment. Tick marks are at 5-km intervals. Times are in minutes:seconds (mm:ss) after 0000:00 UTC 21 May 1998.

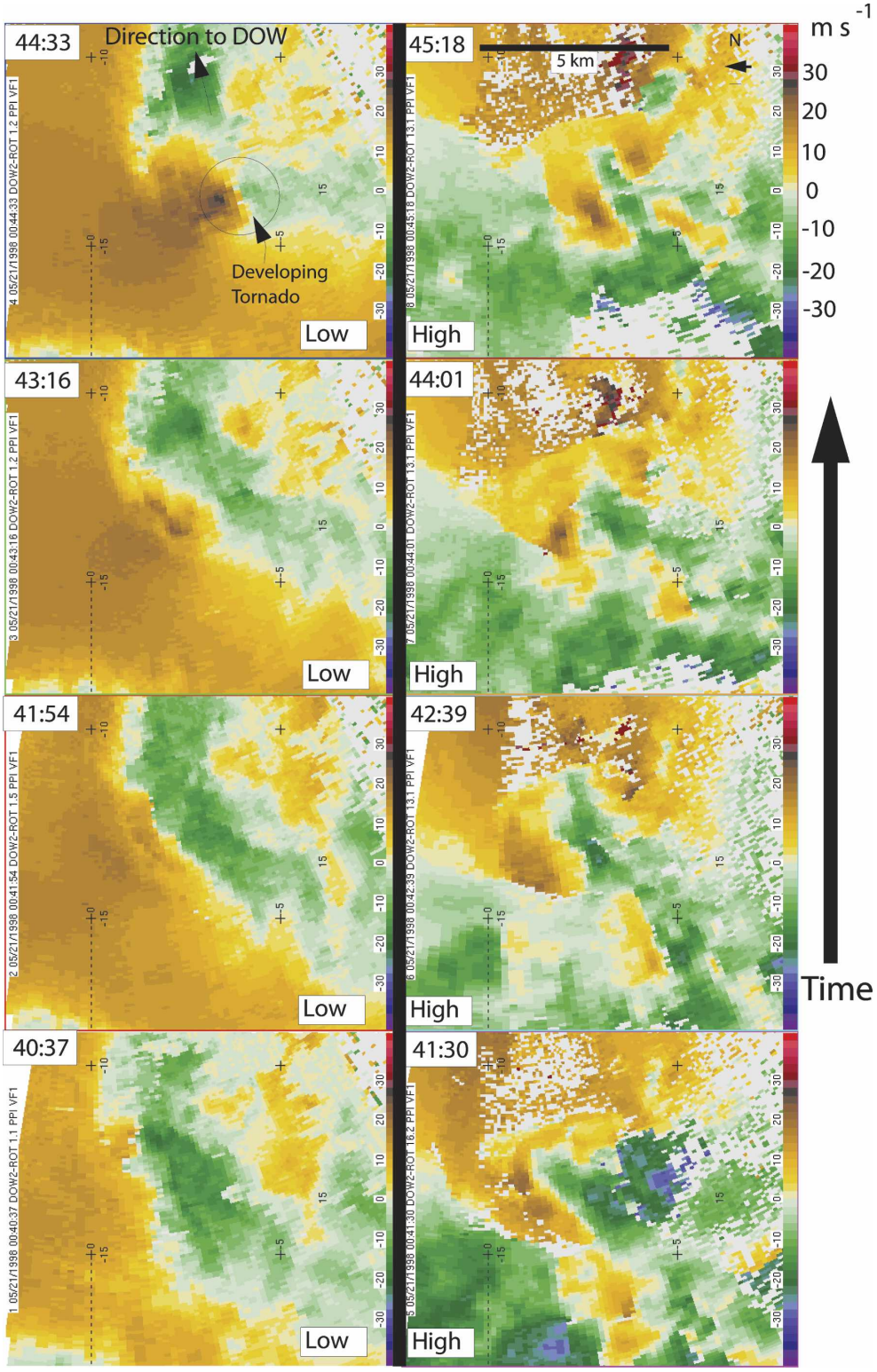


FIG. 4. Low-level and midlevel velocity evolution during tornadogenesis. Scans through the developing tornado at approximately (left) 1.2°–1.5° and (right) 13°–16° elevation reveal the complex evolution of the low- and midlevel velocity field of the tornado, which is finally evident at 0044:33 UTC as indicated by the black circle. Tick marks are at 5-km intervals. Times are in mm:ss after 0000:00 UTC 21 May 1998. The Doppler velocity key is in the top-right panel.

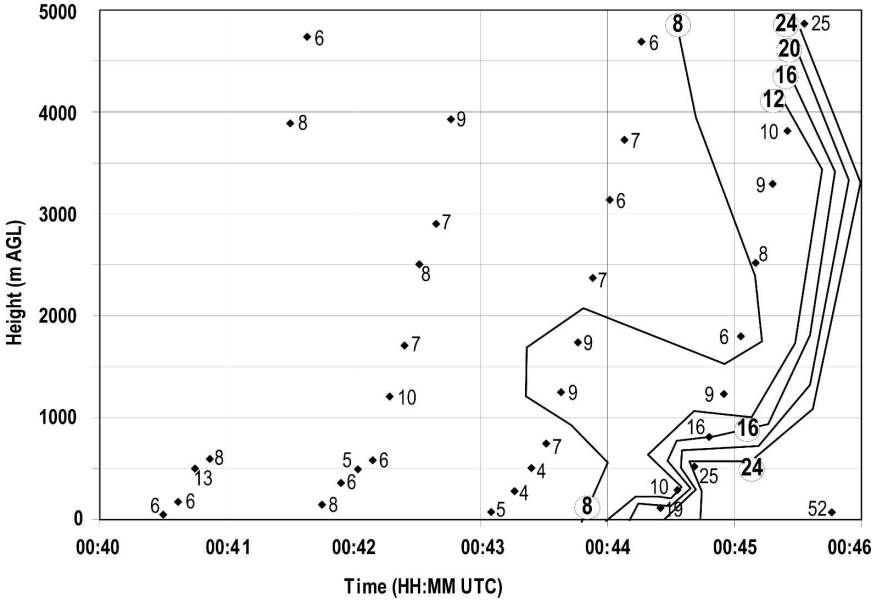


FIG. 5. Evolution of estimated axisymmetric vertical vorticity in developing tornado. Values are $\times 10^{-3}$ s$^{-1}$. Contours are drawn at 0.008, 0.012, 0.016, 0.020, and 0.024 s$^{-1}$. Vorticity develops very rapidly after 0044 UTC, particularly at low levels.

results in vertical vorticity of 0.25 s$^{-1}$. The sudden increase of vorticity at low levels without prior intensification or descent from aloft may not be consistent with some tornadogenesis mechanisms that involve downward propagation of intense rotation (e.g., some of those proposed in Trapp and Davies-Jones 1997). The decay of organized structure and the disappearance of the inferred downdraft above 1 km AGL suggest that this weak tornado formed as a result of an impulsive, as opposed to persistent, process. The coiled reflectivity structure associated with the tornado, even at the moment of genesis, resembles that observed in occluded and dissipating tornadoes (e.g., Wurman and Gill 2000). The gust front of the supercell is well to the east of the tornado, which is also typical of dissipating, not forming, tornadoes.

DOW3 deploys 9.40 km to the south of DOW2 (Fig. 2), and commences scanning at 0046:06 UTC. The tornado is approximately 15 km from each of the DOWs, and the beam-crossing angle of the radars, at the tornado, is 36°, sufficiently large for accurate dual-Doppler analysis. Critical for accurate dual-Doppler retrieval, the two DOWs are precisely leveled during the deployment to within 0.2°.

While deployed in this dual-Doppler configuration, the DOWs conduct single-sector volume-type scans through approximately 140° azimuthally at the following nominal elevations: 0.5°, 1.2°, 2.2°, 3.2°, 5.2°, 7.2°, 10.2°, 13.1°, 16.2°, and 20.2°. Scan rates of about 20°–30° s$^{-1}$ result in sweeps every 5–7 s so the volume requires approximately 1 min to complete. Processing with 0.5-$\mu$s gates using a 0.5-$\mu$s transmit pulse results in 75-m range resolution. Pulse-pair processing produced 32 integrated beams per second, resulting in azimuthal oversampling by a factor of 1.3, which helps enhance azimuthal resolution (Wood et al. 2001) limited by the 250-m radar beam widths at the range of the tornado. The pulse repetition frequency of both DOWs is 2000 Hz, resulting in a Nyquist interval of 32 m s$^{-1}$ and velocity aliasing at values exceeding $\pm 16$ m s$^{-1}$. The result of these data collection modes are three-dimensional fields of Doppler velocities through the tornado and surrounding storm, with radar data spacing near the tornado of approximately 75 m (range) $\times$ 200 m (horizontal) $\times$ 250 m (vertical) or $4 \times 10^7$ m$^3$. Data are manually dealiased and values where the normalized coherent power is less than 0.25 are eliminated. Data contaminated by ground clutter are manually eliminated. Using common radar clutter targets, the DOW data are correctly oriented to within 0.5°. Data from each radar are then interpolated onto a grid with spacing of 100 m in the horizontal and 200 m in the vertical. Cressman interpolation with a horizontal radius of influence of 400 m and a vertical radius of influence of 600 m is used to preserve structures larger than the tornado itself while remaining consistent with the scale of the actual observations as described above. All data are adjusted to a common time by subtracting the translational motion of the tornado. This motion is determined by tracking the reflectivity eye in the center

of the tornado at several times and heights. An average translational velocity is then computed and assumed to be constant over the domain.

After all data have been interpolated onto the Cartesian grid, a dual-Doppler analysis is performed using a two-step, second-order Lax–Wendroff scheme (Sperow et al. 1995) to obtain vertical motion $w$ via upward integration of mass continuity on a grid that is staggered in the vertical. This scheme has been shown to be more accurate than the traditional iterative solution method (Sperow et al. 1995). Data are included only in regions where the between-beam angle is greater than 25° and less than 155°.

At 0046 UTC, the tornado is visible in the low-level scans from both DOWs (Fig. 6). DOW2, which is scanning more slowly, resulting in finer interbeam spacing, measures peak Doppler velocities of 35 m s$^{-1}$ at 70 m AGL with a $\Delta V$ of 61 m s$^{-1}$ across 235 m, resulting in an estimated vertical vorticity of 0.52 s$^{-1}$. DOW3, scanning through the same level 20 s later, measured a $\Delta V$ of only 43 m s$^{-1}$. This difference is likely due to a combination of coarser azimuthal sampling, difficulties dealiasing the DOW3 data in the tornado itself, and actual weakening in the tornado between the DOW2 observations (0045:46 UTC) and DOW3 observations (0046:06 UTC). A gust front extends from north of the tornado eastward, then southward, crossing the latitude of the tornado 10 km east of the tornado.

The dual-Doppler analysis reveals several important features of the tornadic storm and supercell with unprecedented observational detail. Critically, data in three dimensions permits the calculation of horizontal vorticity, the tilting of horizontal vorticity, and the stretching of vertical vorticity. This analysis has not been possible with previous two-dimensional dual-Doppler DOW datasets (Wurman et al. 2007a). The rear-flank downdraft, gust front, and other structures near the tornado having horizontal scales of or exceeding approximately 500–1000 m are well resolved (Carbone et al. 1985) in the DOW data and analysis. The core flow of the tornado, with a diameter of approximately 200 m or less, is not.

The structure of the tornadic region of the storm is similar in many respects to conceptual models (e.g., Lemon and Doswell 1979) and to computer simulations (e.g., Wicker and Wilhelmson 1995; Adlerman et al. 1999; Adlerman 2003) as discussed later. The tornadic rotation at the lowest resolved level is captured in the vector wind field at 100 m AGL. A region of divergence and downward motion comprising the rear-flank downdraft (RFD) extends from the south of the tornado, wrapping around to the east and north (Fig. 7a). The nearly complete wrapping of the RFD around the tornado suggests that the storm system is occluded, possibly cutting off the surface inflow into the tornado. This type of complete occlusion is typical of a soon to dissipate tornado (Wicker and Wilhelmson 1995; Wurman et al. 2007a) and, in fact, this tornado dissipated shortly after the dual-Doppler scans ($\Delta V$ as measured by DOW2 at 0047 UTC was only 51 m s$^{-1}$, and it continued to lessen). Peak values of divergence near the tornado are 0.026 s$^{-1}$. Convergence and upward motion are observed in and to the immediate north of the tornado, with peak values of convergence reaching 0.050 s$^{-1}$. The tornado is located near the boundary between the upward- and downward-moving air. Another region of convergence, with peak magnitude between 0.02 and 0.03 s$^{-1}$, is associated with the gust front (e.g., Brandes 1977, 1978, 1984a,b), well separated from the tornado to the north and east.

Strong cyclonic vertical vorticity, up to 0.11 s$^{-1}$ is associated with the tornado, with values over 0.04 s$^{-1}$ along the gust front to the northeast (Fig. 7c). Note that these are substantially smaller than those calculated from the raw single-Doppler fields (values of 0.2 s$^{-1}$ and even one of 0.52 s$^{-1}$ are shown in Fig. 5) due to the smoothing of the radar data during the gridding process and the inability of the dual-Doppler analysis to resolve the inner-core flow region of the tornado. Anticyclonic vertical vorticity is observed to the east of the tornado and is associated with the region of observed tilting of horizontal vorticity by the RFD (discussed later). No subsequent tornadogenesis occurred near the region of enhanced cyclonic vorticity associated with the gust front. This observation is in contrast to some simulations (e.g., some in Adlerman et al. 1999) and some high-resolution observational analyses of tornadoes (Wurman et al. 2007a), but the detailed mechanisms of cyclic tornadogenesis are not well enough understood to state whether the lack of subsequent genesis in this case is surprising.

There is no significant anticyclonic vertical vorticity observed in the RFD region to the south of the tornado. The fields of vertical vorticity and horizontal divergence in the previously described features are qualitatively similar throughout the depth of the analysis volume, up to 1100 m AGL. The horizontal divergence and vertical vorticity fields at 300 m AGL are shown in Figs. 7b,d.

The vorticity budget of a nonsupercell tornado was analyzed in Roberts and Wilson (1995). Here, for the first time, dual-Doppler data permit stretching and tilting terms in the vorticity budget of a supercell tornado to be calculated with finescale spatial resolution. Stretching of cyclonic vertical vorticity is observed in

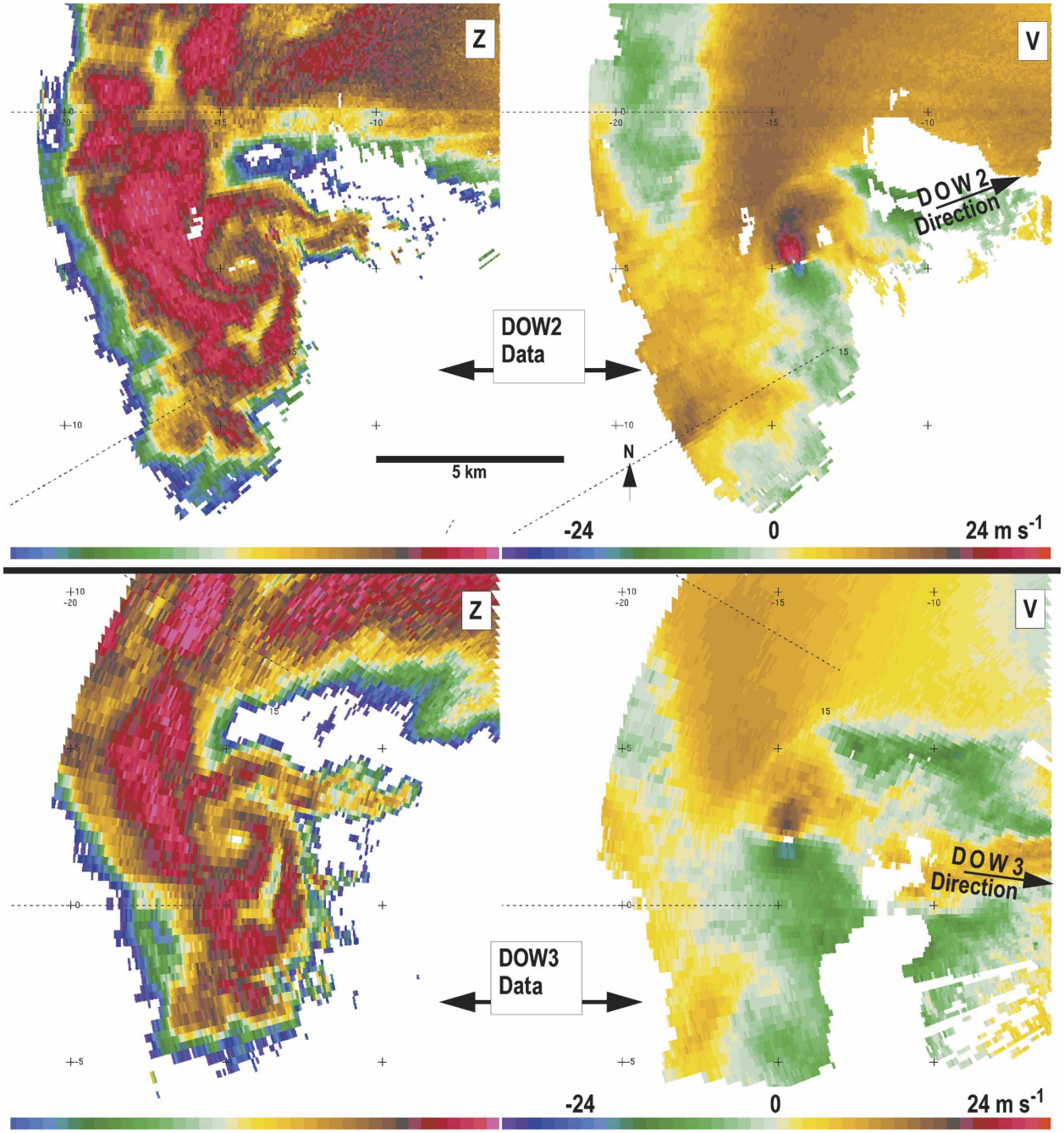


FIG. 6. Tornado as seen by each radar during dual-Doppler deployment from 0045 to 0046 UTC. (left) Uncalibrated reflectivity and (right) Doppler velocity fields reveal a clear central eye and complex surrounding hook echo as well as the small-scale velocity couplet of the weak but distinct tornado. (top) DOW2 and (bottom) DOW3 data. Tick marks are at 5-km intervals.

the tornado throughout the lowest kilometer AGL, while compression of cyclonic vertical vorticity is observed in the RFD region immediately to the south and southeast of the tornado (Figs. 8a,b). Peak positive and negative values, associated with the convergent updraft and divergent RFD, respectively, are near $4 \times 10^{-4}$ s$^{-2}$ in the immediate vicinity of the tornado. This is in close agreement with values of $5 \times 10^{-4}$ s$^{-2}$ found in Adlerman et al. (1999), but less than those found by Wicker and Wilhelmson (1995). Stretching of cyclonic vertical vorticity is also observed in the gust front region to the northeast of the tornado.

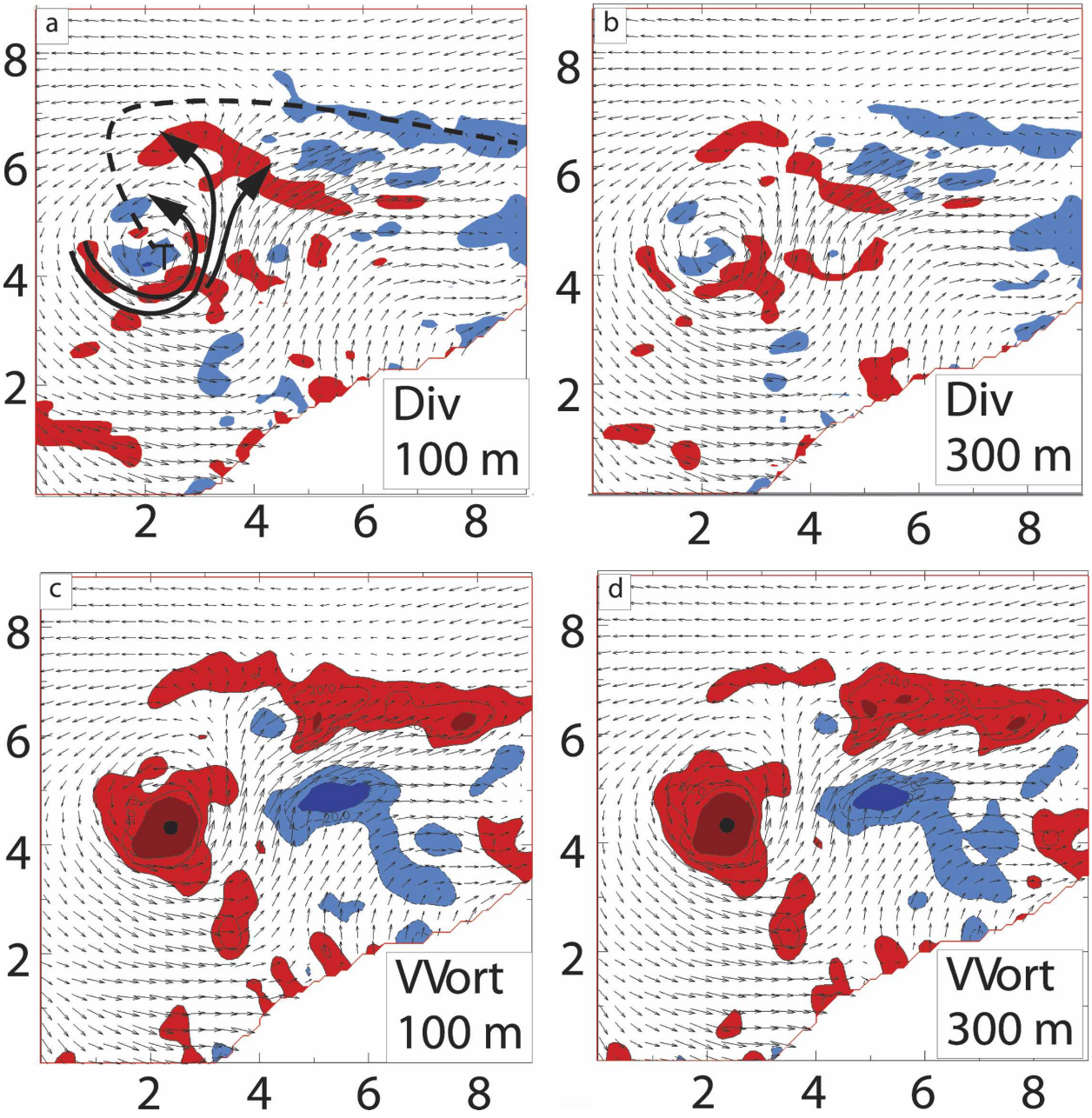


FIG. 7. Dual-Doppler horizontal winds (vectors), horizontal divergence, and vertical vorticity near a supercell tornado. Horizontal component of divergence (red) and convergence (blue) at (a) 100 and (b) 300 m AGL. Vertical component of cyclonic (red) and anticyclonic (blue) vorticity at (c) 100 and (d) 300 m AGL. For reference, approximate locations of tornado (T), RFD (solid lines), and gust front (dash lines) are indicated in (a). Axis labels are in km.

Vertical motion $w$ is calculated by vertically integrating horizontal divergence using a boundary condition of $w = 0$ at the ground, and likely intense horizontal divergence/convergence is not resolved below 100 m AGL. As a result, the magnitude of vertical motion is underestimated at low levels, deleteriously impacting the calculation of both horizontal vorticity and its tilting. Spatially coherent structures in the field of tilting of horizontal vorticity into the vertical are observed at and above 700 m AGL (Fig. 8c) at the boundary between the RFD and the upward-moving air associated with the tornado. Peak values of tilting of horizontal vorticity near the tornado are approximately $4 \times 10^{-4}$ s$^{-2}$. This is in reasonably close agreement with values found in Adlerman et al. (1999) $5 \times 10^{-4}$ s$^{-1}$, and Wicker and Wilhelmson (1995) $1 \times 10^{-4}$ s$^{-2}$. Higher values are

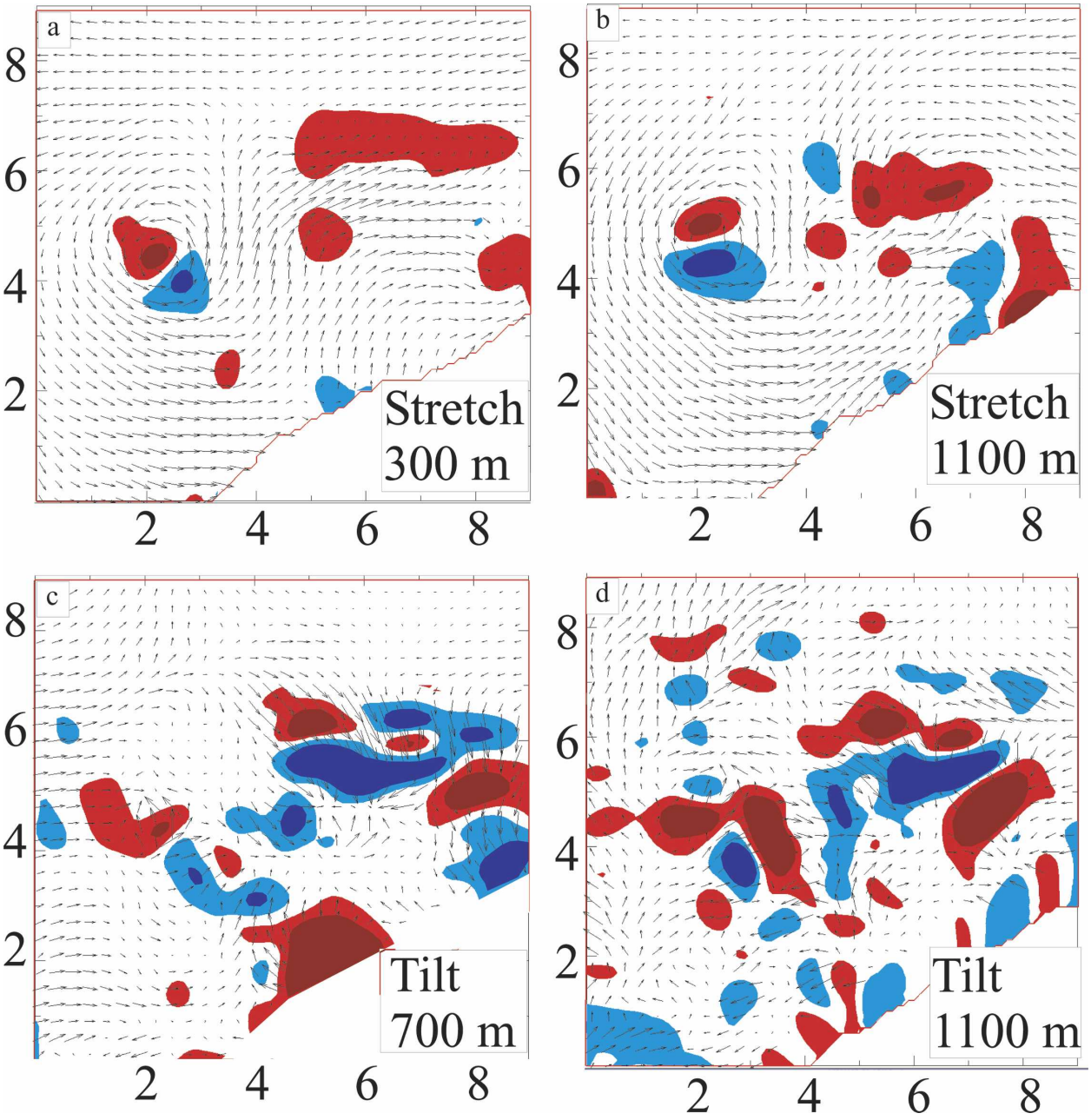


FIG. 8. Dual-Doppler horizontal winds (vectors) and vertical vorticity generation terms near a supercell tornado. Stretching or compression of vertical vorticity into cyclonic (red) or anticyclonic (blue) vertical vorticity at (a) 300 and (b) 1100 m AGL. Tilting of horizontal vorticity into cyclonic (red) or anticyclonic (blue) vertical vorticity at (c) 700 and (d) 1100 m AGL. Axis labels are in km.

found elsewhere, but the horizontal vorticity field appears to be less reliable in those regions. Because trajectory analysis is not possible, it is not provable from this analysis that any air parcels experiencing this tilting are later transported into the tornado. However, it is plausible that parcels would spend up to $10^2$ s in the 1–2-km scale regions where the combined tilting of horizontal vorticity and stretching of vertical vorticity approach $10^{-3}$ s$^{-2}$, and then enter the tornado. Vertical vorticity generation through those processes could then approach $10^{-1}$ s$^{-1}$, which is in reasonably close agreement to the observed 0.2–0.52 s$^{-1}$, particularly because the vorticity generation terms cannot be calculated below 100 m AGL, where significant stretching and tilting likely occur. The horizontal vorticity field appears to be quite disorganized, particularly at 1100 m AGL (Fig.

8d). The appearance of this field is in contrast to that simulated in Alderman et al. (1999), but the tornado observed here was weak and dissipating. However, their simulations show that the strongest tilting is present at low altitudes, near 100 m AGL, a region that was unobservable by the DOWs in this case. Thus, agreement between the observations and their fields is not necessarily expected. In addition, horizontal vorticity is particularly difficult to diagnose using actual data since it is especially sensitive to errors in both vertical and horizontal wind field analyses. While trajectories cannot be calculated using this dataset, the existence and location of the regions in which tilting of horizontal vorticity to the vertical and stretching of vertical vorticity occur are consistent with the tilting then stretching conceptual model of generating intense vertical vorticity associated with tornadoes.

Using the vector wind fields, the total circulation in the region surrounding the tornado is calculated (Fig. 9). The amount of circulation, calculated at a radius of 1.4 km from the tornado center, decreases with increasing altitude, from a value of nearly $4 \times 10^5$ m$^2$ s$^{-1}$ near the ground to below $3.4 \times 10^5$ m$^2$ s$^{-1}$ at 2 km AGL. These values are in remarkable agreement with those found in the numerical simulations of Wicker and Wilhelmson (1995), who found values of $2.0–2.5 \times 10^5$ m$^2$ s$^{-1}$. The numerically simulated values typically decreased with increasing altitude from 0 to 2000 m AGL, consistent with the current observational analysis. The currently analyzed values are 3 times higher than those found in another DOW-observed tornado (Wurman et al. 2007a). It is likely that this is due to natural variation among different tornadoes.

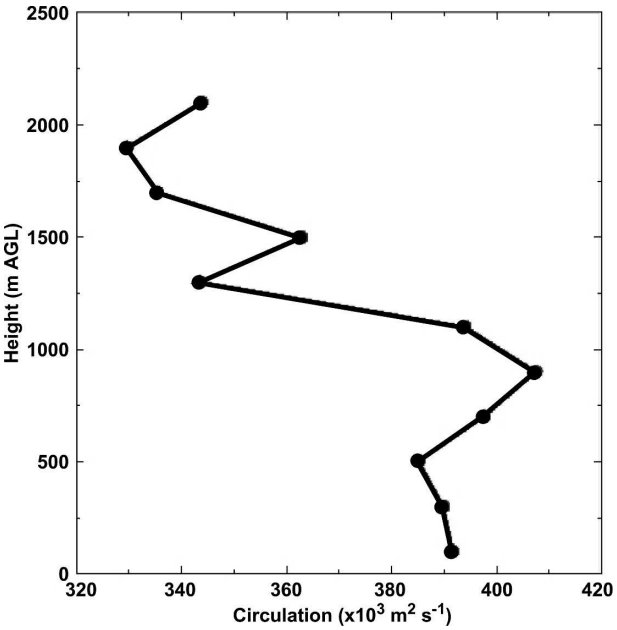


FIG. 9. Circulation vs height in vicinity of tornado around 0045 UTC.

## 4. Conclusions

High-resolution volumetric dual-Doppler data from the DOW mobile radars are used to resolve structures associated with a short-lived and weak tornado. Important terms in the vertical vorticity budget in the region of the tornado are calculated, namely, the tilting of horizontal vorticity and stretching of vertical vorticity. The results agree with some of the predictions of both conceptual and numerical models of tornado formation and maintenance. In particular, tilting of horizontal vorticity at the boundary between the RFD and the updraft, along with stretching of vertical vorticity in the immediate vicinity of the tornado, are consistent with conceptual and numerical predictions. Because the dual-Doppler data exist for only one time, trajectories cannot be calculated, so the actual changes in vorticity of parcels associated with the tilting and stretching terms cannot be diagnosed. However, the magnitude and location of the observed regions of tilting of horizontal vorticity and stretching of vertical vorticity suggest that these mechanisms were adequately resolved and sufficient to generate the vertical vorticity observed in this tornado.

This tornado was weak and short lived. It is possible that the processes necessary for the generation and maintenance of stronger and longer-lived tornadoes are quite different than those involved with the creation of weak and transient ones. While significant magnitudes of vertical and horizontal vorticity, tilting of horizontal vorticity, and stretching of vertical vorticity are observed very near to this tornado, the amplitudes of these fields away from the tornado are much weaker. This suggests that the source of the vertical vorticity for this tornado may be weak or transient, perhaps associated with the short-lived downdraft observed by DOW2 prior to tornadogenesis. The location of the gust front, well away and ahead of the tornado, likely contributes to the rapid occlusion of the inflow region by cutting off any vigorous supply of buoyant air.

The genesis of this weak and short-lived tornado is very rapid and occurs largely during the ~60-s time period necessary to complete one volumetric radar scan (Figs. 3 and 4). To observe these rapid processes, recently developed rapid scan radars (Wurman and Randall 2001) must be used.

*Acknowledgments.* The authors acknowledge Herb Stein, David Dowell, and Swarn Gill, who along with

two of the authors (Wurman and Weygandt) crewed the DOWs during these difficult intercepts. This work was supported by National Science Foundation Grants 0437505, 0437512, 0437898, and NSF CAREER Grant 9703032. The DOW radars were constructed with significant support and assistance from the National Center for Atmospheric Research and the National Severe Storms Laboratory and are operated by the Center for Severe Weather Research with support from the National Science Foundation.

## REFERENCES

Adlerman, E. J., 2003: Numerical simulations of cyclic storm behavior: Mesocyclogenesis and tornadogenesis. Ph.D. dissertation, University of Oklahoma, 217 pp. [Available from School of Meteorology, University of Oklahoma, 100 East Boyd, Suite 1310, Norman, OK 73019.]

——, K. K. Droegemeier, and R. P. Davies-Jones, 1999: A numerical simulation of cyclic mesocyclogenesis. *J. Atmos. Sci.,* **56,** 2045–2069.

Alexander, C. R., and J. Wurman, 2005: The 30 May 1998 Spencer, South Dakota, storm. Part I: The evolution and environment of the tornadoes. *Mon. Wea. Rev.,* **133,** 72–96.

Bluestein, H. B., and A. L. Pazmany, 2000: Observations of tornadoes and other convective phenomena with a mobile, 3-mm wavelength, Doppler radar: The spring 1999 field experiment. *Bull. Amer. Meteor. Soc.,* **81,** 2939–2951.

——, and S. G. Gaddy, 2001: Airborne pseudo-dual-Doppler analysis of a rear-inflow jet and deep convergence zone within a supercell. *Mon. Wea. Rev.,* **129,** 2270–2289.

——, C. C. Weiss, and A. L. Pazmany, 2003: Mobile Doppler radar observations of a tornado in a supercell near Bassett, Nebraska, on 5 June 1999. Part I: Tornadogenesis. *Mon. Wea. Rev.,* **131,** 2954–2967.

——, ——, M. M. French, E. M. Holthaus, R. L. Tanamachi, S. Frasier, and A. L. Pazmany, 2007: The structure of tornadoes near Attica, Kansas, on 12 May 2004: High-resolution, mobile, Doppler radar observations. *Mon. Wea. Rev.,* **135,** 475–506.

Brandes, E. A., 1977: Gust front evolution and tornado genesis as viewed by Doppler radar. *J. Appl. Meteor.,* **16,** 333–338.

——, 1978: Mesocyclone evolution and tornadogenesis: Some observations. *Mon. Wea. Rev.,* **106,** 995–1011.

——, 1981: Finestructure of the Del City-Edmond tornadic mesocirculation. *Mon. Wea. Rev.,* **109,** 635–647.

——, 1984a: Relationships between radar-derived thermodynamic variables and tornadogenesis. *Mon. Wea. Rev.,* **112,** 1033–1052.

——, 1984b: Vertical vorticity generation and mesoscyclone sustenance in tornadic thunderstorms: The observational evidence. *Mon. Wea. Rev.,* **112,** 2253–2269.

——, R. P. Davies-Jones, and B. C. Johnson, 1988: Streamwise vorticity effects on supercell morphology and persistence. *J. Atmos. Sci.,* **45,** 947–963.

Burgess, D., M. Magsig, J. Wurman, D. Dowell, and Y. Richardson, 2002: A detailed WSR-88D and DOW radar analysis of the Oklahoma City tornado of 3 May 1999. *Wea. Forecasting,* **17,** 456–471.

Carbone, R. E., M. J. Carpenter, and C. D. Burghart, 1985: Doppler radar sampling limitation in convective storms. *J. Atmos. Oceanic Technol.,* **2,** 357–361.

Dowell, D. C., and H. B. Bluestein, 1997: The Arcadia, Oklahoma, storm of 17 May 1981: Analysis of a supercell during tornadogenesis. *Mon. Wea. Rev.,* **125,** 2562–2582.

——, and ——, 2002a: The 8 June 1995 McLean, Texas, storm. Part I: Observations of cyclic tornadogenesis. *Mon. Wea. Rev.,* **130,** 2626–2648.

——, and ——, 2002b: The 8 June 1995 McLean, Texas, storm. Part II: Cyclic tornado formation, maintenance, and dissipation. *Mon. Wea. Rev.,* **130,** 2626–2648.

——, Y. P. Richardson, and J. Wurman, 2002: Observations of the formation of low-level rotation: The 5 June 2001 Sumner County, Kansas, storm. Preprints, *21st Conf. on Severe Local Storms,* San Antonio, TX, Amer. Meteor. Soc., CD-ROM, 12.3.

Fujita, T. T., 1975*:* New evidence from the April 3-4, 1974 tornadoes. Preprints, *Ninth Conf. on Severe Local Storms,* Norman, OK, Amer. Meteor. Soc., 248–255.

——, and R. M. Wakimoto, 1982: Anticyclonic tornadoes in 1980 and 1981. Preprints, *12th Conf. on Severe Local Storms,* San Antonio, TX, Amer. Meteor. Soc., 213–216.

Jensen, B., T. P. Marshall, M. A. Mabey, and E. N. Rasmussen, 1983: Storm scale structure of the Pampa storm. Preprints, *13th Conf. on Severe Local Storms,* Tulsa, OK, Amer. Meteor. Soc., 85–88.

Klemp, J. B., and R. Rotunno, 1983: A study of the tornadic region within a supercell thunderstorm. *J. Atmos. Sci.,* **40,** 359–377.

——, R. B. Wilhelmson, and P. S. Ray, 1981: Observed and numerically simulated structure of a mature supercell thunderstorm. *J. Atmos. Sci.,* **38,** 1558–1580.

Lee, W.-C., and J. Wurman, 2005: The diagnosed structure of the Mulhall tornado. *J. Atmos. Sci.,* **62,** 2373–2393.

Lemon, L. R., and C. A. Doswell, 1979: Severe thunderstorm evolution and mesocyclone structure as related to tornadogenesis. *Mon. Wea. Rev.,* **107,** 1184–1197.

Ludlam, F. H., 1963: Severe local storms: A review. *Severe Local Storms, Meteor. Monogr.,* No. 27, Amer. Meteor. Soc., 1–30.

Markowski, P. M., J. M. Straka, and E. N. Rasmussen, 2002: Direct surface thermodynamic observations within the rear-flank downdrafts of nontornadic and tornadic supercells. *Mon. Wea. Rev.,* **130,** 1692–1721.

NCDC, 1998: *Storm Data*. Vol. 40, 165 pp.

Rasmussen, E. N., R. E. Peterson, J. E. Minor, and B. D. Campbell, 1982: Evolutionary characteristics and photogrammetric determination of windspeeds within the Tulia outbreak tornadoes 28 May 1980. Preprints, *12th Conf. on Severe Local Storms,* San Antonio, TX, Amer. Meteor. Soc., 301–304.

Ray, P. S., R. J. Doviak, G. B. Walker, D. Sirmans, J. Carter, and B. Bumgarner, 1975: Dual-Doppler observation of a tornadic storm. *J. Appl. Meteor.,* **14,** 1521–1530.

——, C. L. Ziegler, and R. J. Serafin, 1980: Single- and multiple-Doppler radar observations of tornadic storms. *Mon. Wea. Rev.,* **108,** 1607–1625.

——, B. C. Johnson, K. W. Johnson, J. S. Bradberry, J. J. Stephens, K. K. Wagner, R. B. Wilhelmson, and J. B. Klemp,

1981: The morphology of several tornadic storms on 20 May 1977. *J. Atmos. Sci.,* **38,** 1643–1663.

Richardson, Y., D. Dowell, and J. Wurman, 2001: High resolution dual-Doppler analyses of two thunderstorms during the pretornadogenesis and mature tornado stages. Preprints, *30th Int. Conf. on Radar Meteorology,* Munich, Germany, Amer. Meteor. Soc., 295–297.

Roberts, R. D., and J. W. Wilson, 1995: The genesis of three nonsupercell tornadoes observed with dual-Doppler radar. *Mon. Wea. Rev.,* **123,** 3408–3436.

Romine, G., L. J. Wicker, and M. S. Gilmore, 2004: Analysis of simulated supercell tornadogenesis. Preprints, *22d Conf. on Severe Local Storms,* Hyannis, MA, Amer. Meteor. Soc., CD-ROM, 9.1.

Sperow, K. S., H. B. Bluestein, and T. Gal-Chen, 1995: Testing a Doppler analysis method: The two-step, second order Lax-Wendroff scheme. Preprints, *27th Conf. on Radar Meteorology,* Vail, CO, Amer. Meteor. Soc., 296–298.

Stout, G. E., and F. A. Huff, 1953: Radar records Illinois tornadogenesis. *Bull. Amer. Meteor. Soc.,* **34,** 281–284.

Trapp, J. R., 1999: Observations of nontornadic low-level mesocyclones and attendant tornadogenesis failure during VORTEX. *Mon. Wea. Rev.,* **127,** 1693–1705.

——, and R. Davies-Jones, 1997: Tornadogenesis with and without a dynamic pipe effect. *J. Atmos. Sci.,* **54,** 113–133.

Wakimoto, R. M., and C. Liu, 1998: The Garden City, Kansas, storm during VORTEX 95. Part II: The wall cloud and tornado. *Mon. Wea. Rev.,* **126,** 393–408.

——, and H. Cai, 2000: Analysis of a nontornadic storm during VORTEX 95. *Mon. Wea. Rev.,* **128,** 565–592.

Wicker, L. J., and R. B. Wilhelmson, 1995: Simulation and analysis of tornado development and decay within a three-dimensional supercell thunderstorm. *J. Atmos. Sci.,* **52,** 2675–2703.

——, D. Dowell, Y. Richardson, and R. Wilhelmson, 2002: A large eddy simulation of a tornadic supercell: Comparison with observations. Preprints, *21st Conf. on Severe Local Storms,* San Antonio, TX, Amer. Meteor. Soc., 262–263.

Wood, V. T., R. A. Brown, and D. Sirmans, 2001: Technique for improving detection of WSR-88D mesocyclone signatures by increasing angular sampling. *Wea. Forecasting,* **16,** 177–184.

Wurman, J., 2001: The DOW mobile multiple-Doppler network. Preprints, *30th Int. Conf. on Radar Meteorology,* Munich, Germany, Amer. Meteor. Soc., 95–97.

——, 2002: The multiple-vortex structure of a tornado. *Wea. Forecasting,* **17,** 473–504.

——, and S. Gill, 2000: Finescale radar observations of the Dimmitt, Texas (2 June 1995), tornado. *Mon. Wea. Rev.,* **128,** 2135–2164.

——, and M. Randall, 2001: An inexpensive, mobile, rapid-scan radar. Preprints, *30th Int. Conf. on Radar Meteorology,* Munich, Germany, Amer. Meteor. Soc., CD-ROM, P3.4.

——, and C. Alexander, 2005: The 30 May 1998 Spencer, South Dakota, storm. Part II: Comparison of observed damage and radar-derived winds in the tornadoes. *Mon. Wea. Rev.,* **133,** 97–119.

——, J. Straka, and E. Rasmussen, 1996: Fine scale Doppler radar observation of tornadoes. *Science,* **272,** 1774–1777.

——, J. M. Straka, E. N. Rasmussen, M. Randall, and A. Zahrai, 1997: Design and deployment of a portable, pencil-beam, pulsed, 3-cm Doppler radar. *J. Atmos. Oceanic Technol.,* **14,** 1502–1512.

——, Y. Richardson, C. Alexander, S. Weygandt, and P.-F. Zhang, 2007a: Dual-Doppler and single-Doppler analysis of a tornadic storm undergoing mergers and repeated tornadogenesis. *Mon. Wea. Rev.,* **135,** 736–758.

——, C. Alexander, P. Robinson, and Y. Richardson, 2007b: Low-level winds in tornadoes and potential catastrophic tornado impacts in urban areas. *Bull. Amer. Meteor. Soc.,* **88,** 31–46.

Xue, M., 2004: Tornadogenesis within a simulated supercell storm. Preprints, *22d Conf. on Severe Local Storms,* Hyannis, MA, Amer. Meteor. Soc., CD-ROM. 9.6.